Synthesis, Laser Processing and Flame Purification of Nanostructured Carbon

Randy L. Vander Wal[1], Aaron J. Tomasek[1] and Thomas M. Ticich[2]

[1]NCMR c/o NASA-Glenn
M.S. 110-3
21000 Brookpark Rd.
Cleveland OH 44135

[2]Centenary College of Louisiana
Dept. of Chemistry
Shreveport, LA 77134

Corresponding author email address: randy@rvander.grc.nasa.gov

Introduction

Interest in nanostructured carbons is generated by their potential use as intercalation material for Li batteries [1-3], catalyst support material for fuel cells [4, 5], electrode material for supercapacitors [6], and as gas storage media [7]. In recent years, carbon nanotubes have been extensively investigated for these applications [8]. The attributes that best seem to correlate with their performance are their high surface area and hollow channels. Given this criteria, many other forms of carbon may also be suitable in providing a high surface area and/or nanoscale compartments [9]. This investigation is aimed at producing a new type of nanocarbon by laser annealing of preformed carbon nanospheres.

Laser-based processes based on ablation or pyrolysis have been used to produce nanomaterial such as carbon nanotubes [10], fullerenes [11, 12] and inorganic nanoparticles from gas phase precursors [13, 14]. Graphitized carbon blacks [15] and spherical onions [16, 17] have been synthesized through high temperature annealing over extended times in batch processes. In general nanomaterials synthesis can proceed from either a “top-down” approach involving the breakdown of macroscale material or a “bottom-up” approach involving the build up of molecular materials [18]. The former method invariably is energy intensive and likely to generate byproducts and poor yields. However, such processes can generate macroscopic amounts of material. The latter method permits greater design control of the material and higher conversion efficiencies. Quantities via this route however are low and most approaches are not readily scaleable.

Here we present a hybrid approach by transforming a nanomaterial, soot, into another nanomaterial form of carbon. By starting with a low-cost nanomaterial available in bulk, large quantities may be produced. As a uniform nanoscale material, high conversion efficiencies may be achieved. Therein our rationale for the design of this experiment was to a) devise a method for yielding carbon nanoparticles of uniform size in

the starting material, b) implement a means to effect their transformation into a nanostructured carbon and c) realize a process for their purification. The secondary goal was to configure a system whereby each of these goals could be sequentially implemented to realize a continuous process. Each of these steps is described next.

Experimental

A schematic of the experimental setup is shown in Fig. 1. Unless otherwise noted, benzene was used as the fuel for carbon nanoparticle, i.e. soot synthesis. Vapor from benzene was entrained by a He flow of 10 sccm through a bubbler maintained at room temperature. Gases were introduced into an alumina tube though an ultratorr 1/2 inch cross at the furnace tube entrance. Another port of the cross was sealed with a 0.5 cm diameter quartz window to allow entry of the pulsed laser light. The final port of the cross provided for introduction of an auxiliary amount of helium entering the alumina tube at 100 sccm. This allowed control of the benzene concentration and residence time within the furnace and laser beam. The inert and hydrocarbon gases flowed through a 0.6 cm I.D. alumina tube supported by a 1.9 cm I.D. alumina tube. With the furnace temperature maintained at 1250 ^{0}C, as measured in the center of the furnace, pyrolysis and soot formation readily occurred.

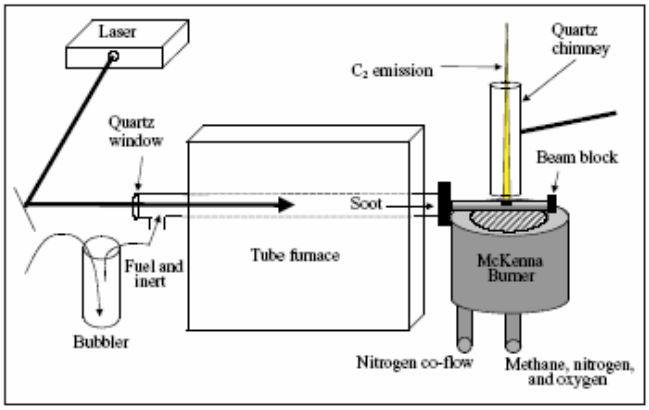

Figure 1.—Experimental schematic illustrating the nanosphere carbon synthesis, laser annealing and flame processing/purification.

The output of the tube was connected to a 3 mm I.D. quartz tube with a 1 mm hole through its sidewall. This tube was positioned across the sintered metal surface of a water cooled McKenna burner with the hole directed upward through the burner center. Through this arrangement, laser heated soot was directed into the post-flame gases of the burner stabilized premixed flame. In comparative experiments, discussed later, nanostructured carbon synthesis using soot derived from ethanol utilized identical conditions except for the following: a) 100 sccm of helium entered the bubbler with no He entering the auxiliary port, compensating for the lower vapor pressure of ethanol. b) The furnace temperature was maintained at 1650 ^{0}C.

Pulsed laser light at 1064 nm and 10Hz was directed into the inner alumina tube by dichroic mirrors. The propagated beam overfilled the alumina tube diameter to provide a near top-hat beam intensity profile throughout the tube. No soot deposition or pyrolysis was observed to occur on the beam entrance window. A beam block at the exit of the quartz tube served as a beam dump. The combination of laser repetition rate and flow rate through the tube allowed several sequential laser pulses to heat the soot during its exit from the furnace. Based on an integrated residence time over the temperature profile from the furnace center to the alumina tube exit, taken as 200 ^{0}C, assuming laminar flow yields an estimate of 10 laser pulses that sequentially heated the soot. We note that as with any process, there will be an inherent limit in process capability. However several

features such as the laser repetition rate, pulse energy, furnace temperature and length can all be scaled upward from the present configuration.

The premixed flame consisted of methane plus a variable percentage of O_2 to create different stoichiometries. A synthetic air mixture of N_2 and O_2 were used with adjustment of the N_2 flow to compensate the O_2 flow in order to maintain a total flow oxidizer flow (N_2 + O_2) of 14.28 slpm. This maintained a nearly constant adiabatic flame temperature and temperature within the chimney of 750 ^{0}C. The methane flow rate was held constant at 1.5 slpm. Flame stoichiometries used in this study were either F = 1.0 or 0.8, the later corresponding to an excess of 20% O_2 in the post-flame gases. A 15 cm long, 2.25 cm I.D. quartz chimney was placed directly above the quartz tube and burner. It served to stabilize the entrained carbon and post-flame gases against buoyancy induced flicker.

Samples of annealed carbon onions were examined by transmission electron microscopy (TEM). TEM samples were collected directly upon lacey TEM grids by thermophoretic sampling directly above the chimney. The TEM was performed in a Phillips CM200 operating at 200 KeV using a LaB6 filament. Gatan software, v. 3.4 was used for microscope operation.

Results

The images shown in Fig. 2 are of the laser treated soot using a fluence of 240 mJ/cm^2, as collected from the flame environment. The action of the laser light is observed as a faceting of the nanocarbons. They exhibit a rosette appearance with somewhat greater transparency relative to non-laser heated soot. We attribute the presence of the non-annealed soot due to warping of the alumina tube creating misalignment of laser relative to the flow axis; thereby allowing some soot to be unheated. Pristine tubes generally eliminated this form of residual carbon. Even so, as the low magnification image shows, the degree of conversion is relatively high, roughly > 75% based on visual inspection of more than 12 such images from different regions on at least two individual samples.

The high magnification image illustrates that this faceting is due to the formation of a chaotic structure within the particles. The structure reflects a reorganization of material within the particle leaving many small voids throughout the interior of the particles. As Fig. 2b shows, some of these voids are centrally located while others are distributed; they appear to extend along boundaries or the particle perimeter. The boundaries defining the empty spaces appear as dark ribbons or bands. These bands have extended lengths of a few nanometers and are organized into nested groupings within the particle. As seen, the size of these voids varies depending upon the arrangement of the ribbons. A variety of widths are observed with the thicker bands appearing along the particle perimeter.

Figure 2c reveals the nature of these bands as being ribbons of carbon layer planes with extended lengths. The number of layer planes, as viewed on-edge varies from 2 to 6. A highly contorted nanostructure is created by their winding within the particle.

The varying tilt of the layer planes relative to the image plane accounts for the differing opacities and clarities of these ribbons partitioning the particle's interiors as seen in the lower magnification image of Fig. 2b.

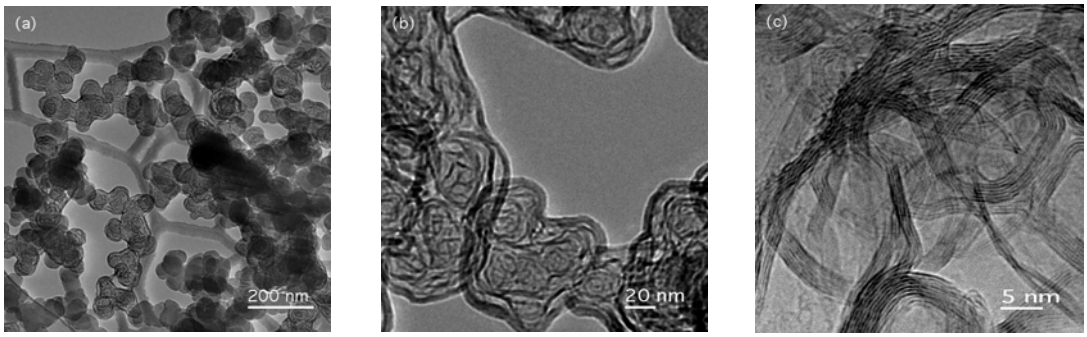

Figure 2 TEM images of flame processed, nanostructured carbon using a laser fluence of 240 mJ/cm^2. Operating near Φ = 1, the flame did not introduce any purification. The lower magnification images illustrate the degree of conversion and morphology of the laser-annealed soot while the higher magnification images reveal the particle nanostructure.

At the higher fluence of 410 mJ/cm^2, the carbon spherules appear to possess greater transparency with a higher definition of internal organization as seen in Fig. 3. The dark bands have become more distinct and appear more continuous. Some of the bands appear to be nested concentric semi-spherical shells while others appear rather random in shape and position within the particles. While the majority of particles are converted into a rosette structure, other structures are also observed. A few hollow capsules, some nested fullerenic structures and very small carbon particles as debris are produced.

The evolution of the rosette structure is seen by comparison of the nanosphere structure displayed in Figs. 3a - 3b to that produced using a lower value of laser fluence of 240 mJ/cm^2 as illustrated in Figs. 2a - 2b. The higher laser fluence creates larger internal voids with a more pronounced definition of internal organization. Thicker ribbons appear to define the internal structure. Some of the particles possess only a few internal cavities, suggesting their evolution towards empty shells. A few shells appear to be formed by the merging of adjacent particles given their elongated shape, though in general the dimensions of the original particles appear to be largely preserved. Finally, the majority of particles are transformed into compartmentalized carbon nanoparticles.

Consistent with the general appearance of the particles in Fig. 3a and 3b, as the higher magnification image of Fig. 3c represents, the compartments have grown larger. Central and perimeter spaces have increased in size by merging, thereby leading to fewer voids. As seen in Fig. 3c, the bands or ribbons have become more extended an increased in width. Their curvature and intersections naturally lead to the partitioning of the particle interiors.

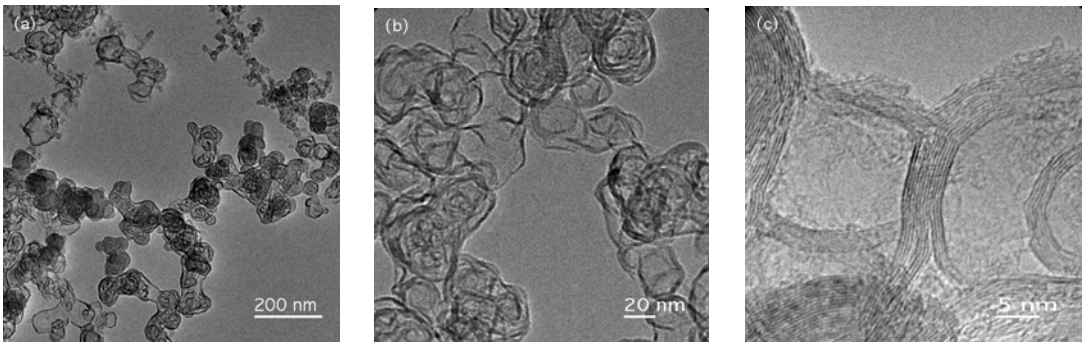

Figure 3 TEM images of flame processed, nanostructured carbon using a laser fluence of 410 mJ/cm^2. Operating at Φ = 1, the flame did not introduce any purification. The lower magnification images illustrate the degree of nanoparticle restructuring (annealing) and variety of products while the higher magnification image illustrates the increased graphitization produced by the pulsed laser annealing using this higher fluence.

Given the greater variety and prevalence of carbon particle forms and sizes, purification is required at this higher fluence (410 mJ/cm^2) to isolate the nanostructured carbon spherules. Figure 4 illustrates the collected soot as processed by the flame using a fuel-air equivalence ratio of 0.8. This corresponds to a lean stoichiometry by virtue of the excess oxygen content of 20%. As shown, the collected aggregates possess the same general appearance and degree of internal structure. In contrast to the laser processed material, no shells, residual small carbon particles or other debris are found. There is no amorphous carbon upon the exteriors of the particles nor shell fragments. Irregular or nonuniform particles are absent. The particles as grouped within the aggregates manifest a similar morphology with a compartmentalized interior.

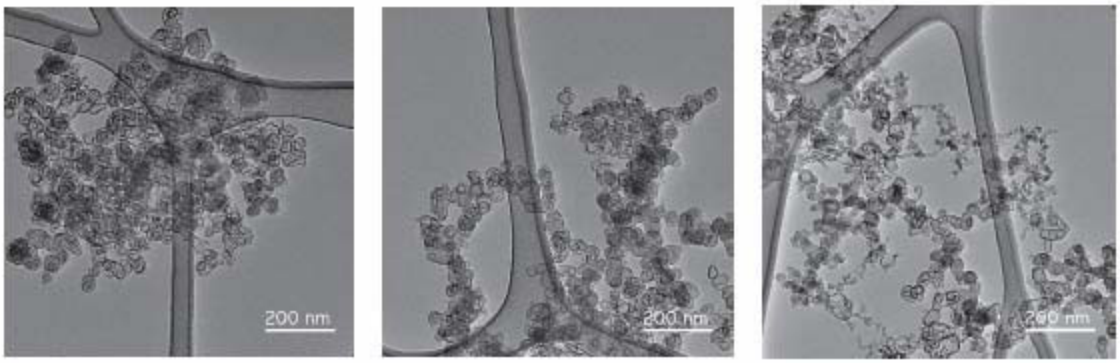

Figure 4 TEM images of flame processed, nanostructured carbon using a laser fluence of 410 mJ/cm^2. The flame, operating at F = 0.8 served to purify the laser annealed carbon through oxidation by removing shells, fragments, ablation products and non-annealed soot. The purification is illustrated by comparison with Fig. 3 illustrating only the original laser heated material sampled from the flame using Φ = 1.0 where no purification by oxidation has occurred.

Figure 5 TEM images of laser processed soot, using a laser fluence of 820 mJ/cm^2. Operating at Φ = 1, the flame introduced no purification. The larger variation in laser produced products at this larger fluence is evident by comparison with Figs. 3 and 4.

At the highest fluence of 820 mJ/cm^2, a very large amount of ultrafine particles and other small structures are produced, as observed in Fig. 5. Such material is characteristic of remnants of ablated material or condensed carbon vapor produced by ablation as observed and reported elsewhere [19]. A wider variety of other structures are also generated such as hollow shells or capsules and fragments thereof with greater prevalence than with the lower fluence of 410 mJ/cm^2 [19]. Some fullerenic structures are also observed. Notably the rosette or compartmentalized structures so apparent in

the lower energy cases are far fewer. Most particles appear to have undergone a transformation into capsules or undergone degradation into ablation products. From the TEM image of Fig. 5, it is clear that higher laser energy is not beneficial. Instead a much larger amount and variety of decomposition products are created.

Discussion

A particular advantage of using the preformed soot is the predefined size and shape of the carbon particles. No breakdown of macroscopic material is required. The initial stage of molecular self-assembly has been completed. Aerosol formation of soot naturally accomplishes this step. This is the most important stage as it determines the size of the particles. Reorganization of the material can then be accomplished using a separate, subsequent process, leading to greater control of the degree of annealing produced through control of the laser fluence. As the images show, different laser fluences produce different structures. The degree of conversion/graphitization will determine the "ideal" value of fluence, (e.g. compare Figs. 2, 3 and 5). As illustrated by Fig. 5, very high fluences produce ablation products which likely will be undesirable for most applications. Therein fluences near this value may represent an upper limit for useful processing.

Use of the material in aerosol form is particularly advantageous for continuous laser processing and entrainment into the flame environment. An additional benefit is that the particle, in aerosol form, possesses a maximum exposed surface area for etching of any amorphous carbon and processing. This uniform isolation of the restructured carbon nanoparticles constitutes a purification and thereby demonstrates the capability of a flame as a separation technique for purification of graphitic material. Control of the flame stoichiometry provides direct control of the oxidation conditions for purification.

Flame Purification/Cleaning

The contrast between the images in Fig. 3 and those in Fig. 4 of the flame processed carbon illustrates the purification provided by the flame. In the purified carbon, no amorphous carbon, unconverted particles, shell or capsule fragments, fullerenic or ablation debris are observed. These byproducts possess a greater number of edge site carbon atoms relative to those within basal plane sites. As is well known for graphite and graphite-like materials, the reactivity of carbon atoms in edge site positions is far greater than those within basal plane positions [20-26]. Moreover, the curvature of the carbon segments within the debris further increases its reactivity by introducing bond strain [27, 28]. This differential reactivity is exploited in the selective oxidation of the amorphous carbon while the graphitic carbon, comprising the annealed particles, remains in tact.

We note that the rate of oxidation is highly dependent upon temperature, oxidizing species identity, their concentrations and time. Therein the flame gases offer an appealing environment where each of these variables may be controlled. The temperature of the post-flame gases can be varied by the choice of fuel, fuel-air stoichiometry and by the addition of gases, such as inerts. The gas composition can be further adjusted through the fuel-air equivalence ratio of the flame and by substitution of oxygen for nitrogen to further increase its concentration within the post-flame gases while

maintaining the same temperature. Buoyancy acts favorably upon the reacting flow of flame gases and nanostructed carbon by restricting the reaction time to 10's of milliseconds thereby minimizing degradation of the graphitic carbon [29]. Finally the flame process is ideally suited towards aerosol processing, thereby laying a foundation for continuous and scaleable operation.

Mechanism of Graphitization

From these images presented in Figs. 2-4 the trend of increasing material reorganization with increasing laser fluence is clear. The relationship between laser fluence and degree of annealing reflects a combination of the peak temperature to which the soot is heated and its duration at elevated temperature [30]. The former is controlled by the absorbed energy which scales with incident laser fluence. The latter is determined by the difference between the initial temperature to which the soot is heated and the furnace temperature. Together, these determine the rate of cooling by conduction.

The restructuring of the soot is enabled by bond breaking and reforming [31-35]. Amorphous carbon can become joined to lamella to extend their length, or it can be vaporized. Neighboring graphitic segments can also bond to grow in length. Their relative orientation will determine the direction of the evolving ribbon. Cross links between lamella may break allowing reorientation into more energetically favored positions and orientations. As the graphitic bands form, they can provide a template against which further carbon restructuring can occur. As internal carbon is consumed in this process, voids are left. Restructuring of carbon along graphitic bands, particularly along the particle perimeter accounts for the nonspherical, elongated vacancies. Higher temperatures, generated by higher laser fluences create more ordered nanostructure. This occurs because of greater fluidity of the carbon segments to reorient and join, in concert with a longer time duration at elevated temperature. Increasing temperature and time thereby account for the greater degree of annealing or graphitization of the carbon nanospheres. This is manifested by graphitic ribbons with greater length, a larger number of parallel layer planes and consequently larger internal compartments.

Conclusions

Starting from a molecular precursor, carbon nanosphere synthesis, annealing and purification steps are each performed in the aerosol phase. Moreover, by separating the different steps of the process, each is uncoupled from considerations of the following step allowing for its optimization and independent control. By tailoring the fuel and temperature, the initial soot structure can be varied to predispose the annealing process towards a particular nanostructure. Adjusting the laser power governs the degree to which graphitization of the nanospheric carbon occurs. The flame stoichiometry provides the critical step in the purification of the annealed material. Amorphous carbon in the form of small particles and ablation debris is selectively etched/gasified while the graphitic nano-onions remain intact. Fragments of graphitic capsules are also removed. Finally, the aerosol process provides high throughput with continuous processing. Such nanostructured carbon materials are anticipated to find use in many energy storage applications based on their high surface area and nanocompartments.

Acknowledgements

This work was supported by a NASA NRA 97-HEDs-01 combustion award (RVW) administered through NASA cooperative agreement NAC3-975 with The National Center for Microgravity Research on Fluids and Combustion (NCMR) at The NASA-Glenn Research Center. Prof. Ticich and Mr. Leif Sherry acknowledges support through the Ohio Aerospace Institute Collaborative Aerospace program for visiting summer faculty. The authors gratefully acknowledge Leif Sherry (Centenary College of Louisiana) and Gordon M. Berger (NCMR) for assistance with the experiments and Dr. Y. L. Chen and David R. Hull for the TEM imaging.

References

1. Claye AS, Fischer JE, Huffman CB, Rinzler AG, and Smalley RE, J. of The Elect. Chem. Soc. 2000;147:2845.
2. Maurin G, Bousquet Ch, Henn F, Bernier P, Almairac R, and Simon B, Chem. Phys. Lett. 1999;312:14.
3. Lu W, and Chung DDL, Carbon 2001;39:493.
4. Steigerwait ES, Deluga GA, and Lukehart CM, J. Phys. Chem. B 2002;106:760.
5. Rodriquez NM, Kim MS, and Baker RTK, J. Phys. Chem. 1994;98:13108.
6. Frackowiak E, and Beguin F, Carbon 2001;39:937.
7. Dagani R, “tempest in a tiny tube”, C&E News, January 14, 2002 pp. 25-28.
8. Perspectives in Fullerene Nanotechnology, (E. Osawa, Ed.), Kluwer Academic Publishers, Dordrecht, The Netherlands, 2002.
9. Bekyarova E, Kaneko K, Yudasaka M, Murata K, Kasuya D, and Iijima S, Adv. Mater. 2002;14:973.
10. Guo T, Nikolaev P, Thess DT, Colbert DT, and Smalley RE, Chem. Phys. Lett. 1995;243:49.
11. Kasuya D, Kokai F, Takahashi K, Yudasaka M, and Iijima S, Chem. Phys. Lett. 2001;337:25.
12. Alexandrescu R, Armand X, Cauchetier M, Herlin N, Petcua S, and Voicua I, Carbon 1998;36:1285.
13. Suyama Y, Marra RM, Haggerty JS, and Bowen HK, Am. Ceram. Soc. Bull. 1985;64:1356.
14. Cannon WR, J. Am. Ceram. Soc. 1982;65:330.
15. Millward GR, and Jefferson DA, Lattice resolution of carbons by electron microscopy, in “The Chemistry and Physics of Carbon”, (P. L. Walker and P. A. Thrower, Eds.), Marcel Dekker Inc., New York, 1970,Vol. 14, pp. 1-82.
16. Tomita S, Burian A, Dore JC, LeBolloch D, Fujii M, and Hayashi S, Carbon 2002;40:1469.
17. Kuznetsov VL, Chuvilin AL, Butenko YV, Mal’kov IY, and Titov VM, Chem. Phys. Lett. 1984;222:343.
18. WTEC Panel Report on Nanostructure Science and Technology, (R. D. Siegel, et al., Eds.) Kluwer Academic Publishers, Dordrecht, The Netherlands, 2000.
19. Vander Wal RL, Ticich TM, and Stephens AB, Appl. Phys. B 1998;67:115.
20. Smith WR, and Polley MH, J. Chem. Phys. 1956;52:689.
21. Thomas JM, Microscopy studies of graphite oxidation, in The Chemistry and Physics of Carbon, (Walker PL, Jr., Ed.) 1965, Vol. 1, p. 121.

22. Henning GR, Chemistry and Physics of Carbon, (Walker PL, Jr., Ed.), 1966, Vol. 2, p. 1-53.
23. Levy M, and Wong P, J. of The Electrochem. Soc. 1964;11:1088.
24. Rosner DE, and Allendorf HD, AIAA Journal 1968;6:650.
25. Donnet JB, Carbon 1982, 20, 267.
26. Marsh H, Introduction to Carbon Science, Butterworths, London, 1989, Chp. 4, pp. 107-152.
27. Dresselhaus MS, Dresselhaus G, and Eklund PC, Science of Fullerenes and Carbon Nanotubes, Academic Press Inc. 1996.
28. “Carbon Nanotubes, Preparation and Properties”, CRC Press Inc., (Ebbesen TW, Ed.), 1997.
29. Roper FG, Combust. and Flame 1977;29:219.
30. Santoro RJ, and Shaddix CJ, “Laser-Induced Incandescence”, in Applied Combustion Diagnostics (Kohse-Hoinghaus K, and Jeffries JB, Eds.) Taylor and Francis, Great Britain, 2002, Chp. 9, pp. 252-286.
31. Akamatu H, and Kuroda H, Proc. 4th Carbon Conference, Pergamon Press Inc., New York 1960, pp. 355-369.
32. Heckman FA, and Harling DF, Rubber Chem. and Technol. 1966, 39, 1. See also The Presentation at the Annual meeting of the Division of Rubber Chemistry, The American Chem. Soc., Miami Beach.
33. Hess WM, Ban LL, Eckert FJ, and Chirico V, Rubber Chem. and Technol. 1968;41:356.
34. Emmerich FG, Carbon 1995;33:1709.
35. Vander Wal RL, and Choi MY, Carbon 1999;37:231.